Neutrino Physics

Summer 2025

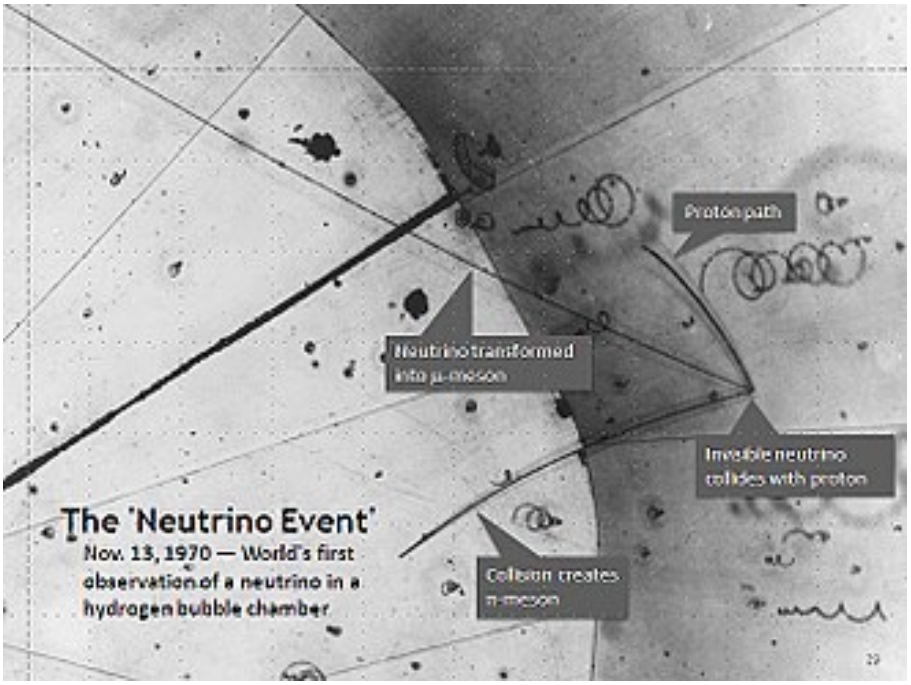

Guru Jahnavi Madana,

Engineering Physics

"Neutrinos alone, among all the known particles, have ethereal properties that are striking and romantic enough both to have inspired a poem by John Updike and to have sent teams of scientists deep underground for 50 years to build huge science-fiction-like contraptions to unravel their mysteries."

— Lawrence M. Krauss

Contents

1 Two-Flavor Neutrino Oscillation Analysis **3**

1.1 Key Equations . . . 3

1.2 Oscillation Probability vs. Pathlength . . . 4

1.3 Oscillation probability vs. Energy . . . 5

2 Three-Flavor Neutrino Oscillation Analysis **9**

2.1 Key Equations . . . 9

2.2 Oscillation probability vs. Pathlength . . . 10

2.3 Oscillation Probabilty vs. Energy . . . 10

2.4 Computational Methodology . . . 12

3 MSW Resonance **13**

3.1 Effective Mixing Angle in Matter vs. Electron Density . . . 13

3.1.1 Computational Methodology . . . 13

3.1.2 Key Equations . . . 14

3.1.3 MSW Mixing Angle Plot . . . 14

3.2 Effective squared masses in matter for neutrinos in the case of two flavor mixing . . . 15

3.2.1 Introduction . . . 16

3.2.2 Theoretical Framework . . . 16

3.2.3 Analysis of the Graph . . . 17

3.2.4 Physical Interpretation . . . 17

3.2.5 Conclusion . . . 18

1. Two-Flavor Neutrino Oscillation Analysis

This section examines two-flavor neutrino oscillations, focusing on the probabilities of $\nu_\mu \to \nu_\tau$ and $\nu_\mu \to \nu_\mu$ transitions as functions of pathlength and neutrino energy. We analyze the effects of varying the mass-squared difference (Δm^2) and mixing angle parameter ($\sin^2 2\theta$) using theoretical plots generated with Python and Matplotlib.

1.1 Key Equations

The oscillation probability for $\nu_\mu \to \nu_\tau$ in a two-flavor vacuum model is given by:

$$P(\nu_\mu \to \nu_\tau) = \sin^2 2\theta \sin^2 \left(\frac{1.27 \Delta m^2 L}{E_\nu} \right), \tag{1}$$

where:

- $\sin^2 2\theta$: Mixing parameter, controlling oscillation amplitude.
- Δm^2: Mass-squared difference (in eV^2).
- L: Pathlength (in km).
- E_ν: Neutrino energy (in GeV).
- The constant 1.27 accounts for unit conversions.

The survival probability is:

$$P(\nu_\mu \to \nu_\mu) = 1 - P(\nu_\mu \to \nu_\tau). \tag{2}$$

The oscillation length, the distance for one complete cycle, is:

$$L_{\text{osc}} = \frac{2.48 E_\nu}{\Delta m^2}. \tag{3}$$

For pathlength dependence, the first maximum of $P(\nu_\mu \to \nu_\tau)$ occurs at:

$$L_{\max} = \frac{\pi E_\nu}{1.27 \Delta m^2}. \tag{4}$$

For energy dependence at fixed L, the first maximum occurs at:

$$E_{\max} = \frac{1.27 \Delta m^2 L}{\pi}. \tag{5}$$

1.2 Oscillation Probability vs. Pathlength

Plots were generated for oscillation probabilities versus pathlength with $E_\nu = 1\,\text{GeV}$ and L ranging from 0 to 10.000 km. The base parameters were $\Delta m^2 = 2.5 \times 10^{-3}\,\text{eV}^2$ and $\sin^2 2\theta = 0.9$. Additional plots tested $\Delta m^2 = 1 \times 10^{-3}\,\text{eV}^2$ and $\sin^2 2\theta = 0.21$.

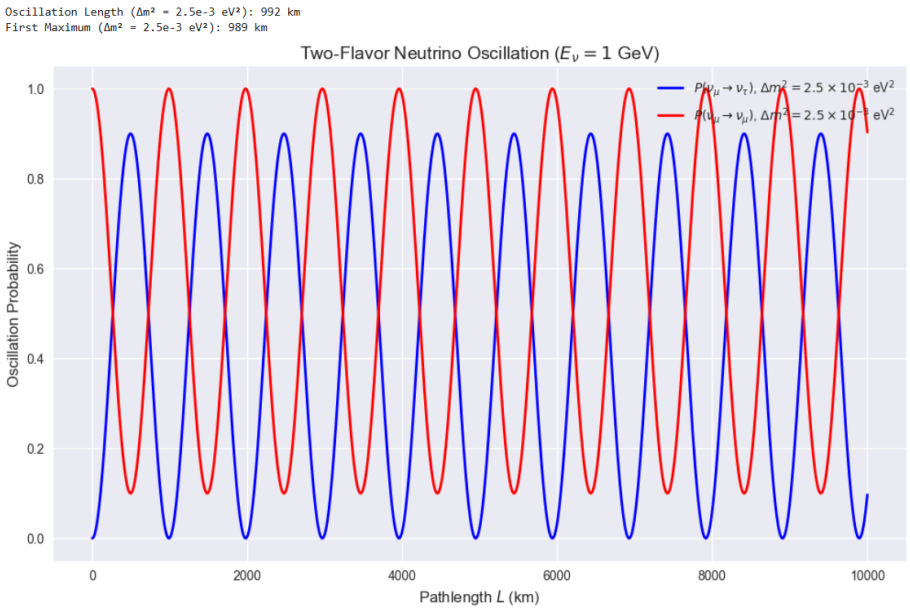

Figure 1: Oscillation probabilities $P(\nu_\mu \to \nu_\tau)$ and $P(\nu_\mu \to \nu_\mu)$ vs. pathlength for $\Delta m^2 = 2.5 \times 10^{-3}\,\text{eV}^2$, $\sin^2 2\theta = 0.9$, $E_\nu = 1\,\text{GeV}$.

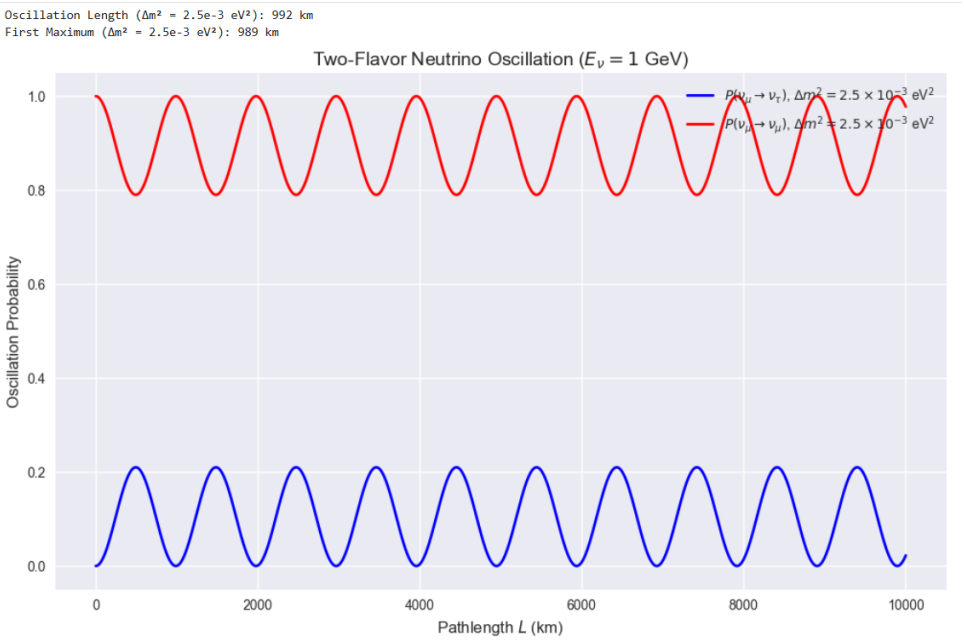

Figure 2: Oscillation probabilities $P(\nu_\mu \to \nu_\tau)$ and $P(\nu_\mu \to \nu_\mu)$ vs. pathlength for $\Delta m^2 = 2.5 \times 10^{-3}\,\text{eV}^2$, $\sin^2 2\theta = 0.21$, $E_\nu = 1\,\text{GeV}$.

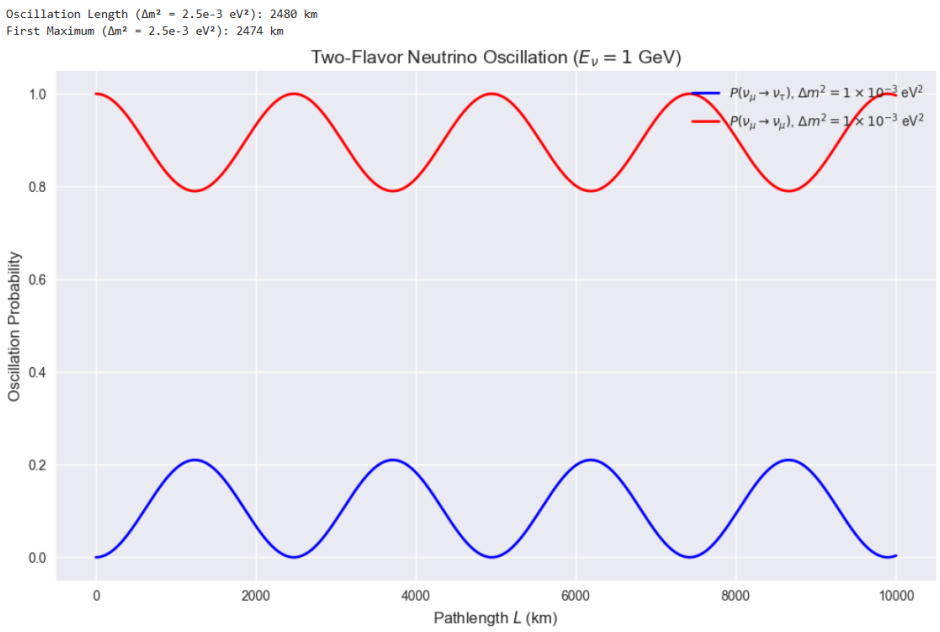

Figure 3: Oscillation probabilities $P(\nu_\mu \to \nu_\tau)$ and $P(\nu_\mu \to \nu_\mu)$ vs. pathlength for $\Delta m^2 = 1 \times 10^{-3}\,\mathrm{eV}^2$, $\sin^2 2\theta = 0.21$, $E_\nu = 1\,\mathrm{GeV}$.

For the base case, the oscillation length is $L_{\mathrm{osc}} \approx 992\,\mathrm{km}$, and the first maximum occurs at $L_{\mathrm{max}} \approx 989\,\mathrm{km}$. The high $\sin^2 2\theta = 0.9$ yields a maximum $P(\nu_\mu \to \nu_\tau)$ of 0.9. Reducing Δm^2 to $1 \times 10^{-3}\,\mathrm{eV}^2$ increases $L_{\mathrm{osc}} \approx 2480\,\mathrm{km}$, stretching the oscillation cycles. Lowering $\sin^2 2\theta$ to 0.21 reduces the maximum probability, affecting amplitude but not frequency.

1.3 Oscillation probability vs. Energy

Plots of oscillation probabilities versus energy were generated for a fixed $L = 1000\,\mathrm{km}$ and E_ν from 0.1 to 10 GeV, using the same parameter sets as above.

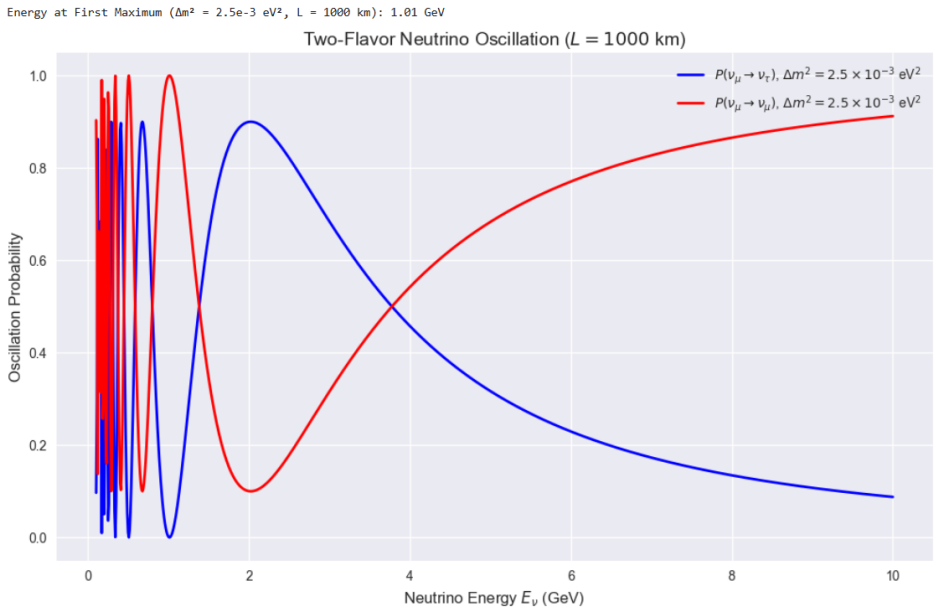

Figure 4: Oscillation probabilities $P(\nu_\mu \to \nu_\tau)$ and $P(\nu_\mu \to \nu_\mu)$ vs. energy for $\Delta m^2 = 2.5 \times 10^{-3}\,\mathrm{eV}^2$, $\sin^2 2\theta = 0.9$, $L = 1000\,\mathrm{km}$.

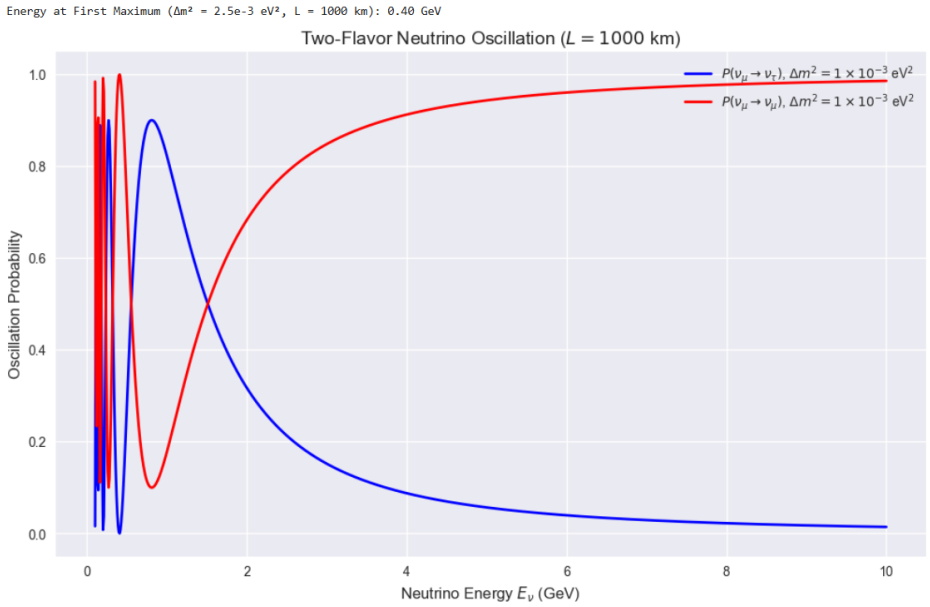

Figure 5: Oscillation probabilities $P(\nu_\mu \to \nu_\tau)$ and $P(\nu_\mu \to \nu_\mu)$ vs. energy for $\Delta m^2 = 1 \times 10^{-3}\,\mathrm{eV}^2$, $\sin^2 2\theta = 0.9$, $L = 1000\,\mathrm{km}$.

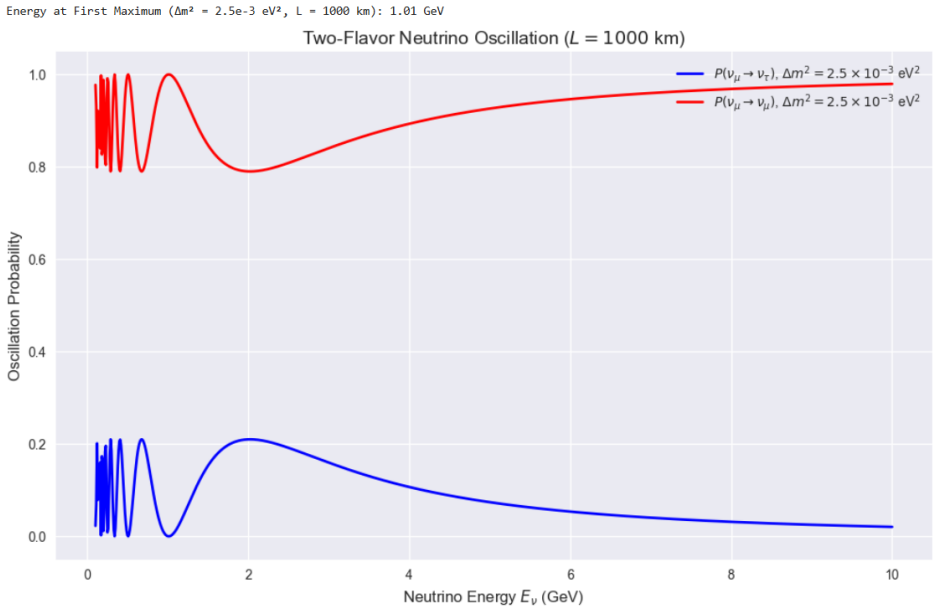

Figure 6: Oscillation probabilities $P(\nu_\mu \to \nu_\tau)$ and $P(\nu_\mu \to \nu_\mu)$ vs. energy for $\Delta m^2 = 12.5 \times 10^{-3}\,\text{eV}^2$, $\sin^2 2\theta = 0.21$, $L = 1000\,\text{km}$.

For the base case, the first maximum is at $E_{\text{max}} \approx 1.01\,\text{GeV}$. Higher energies decrease the oscillation frequency due to the $1/E_\nu$ term in Equation 1. A lower $\Delta m^2 = 1 \times 10^{-3}\,\text{eV}^2$ shifts the maximum to $E_{\text{max}} \approx 0.4\,\text{GeV}$ and slows the oscillations. Reducing $\sin^2 2\theta$ to 0.21 lowers the amplitude.

Physics Behind the Plots

The oscillation probability (Equation 1) depends on:

- $\sin^2 2\theta$: Determines the amplitude. A value of 0.9 maximizes oscillations, while 0.5 halves the maximum probability.
- The phase $\phi = \frac{1.27\Delta m^2 L}{E_\nu}$: Governs the frequency. Larger Δm^2 or L, or smaller E_ν, increases ϕ, leading to faster oscillations.

In pathlength plots, increasing L drives more oscillation cycles, with the period set by L_{osc}. A larger Δm^2 shortens L_{osc}, increasing frequency. In energy plots, higher E_ν reduces the phase, causing faster oscillations. A smaller Δm^2 decreases the frequency, shifting maxima to lower energies. These dependencies guide neutrino experiment design, optimizing L and E_ν for maximum sensitivity.

Varying Δm^2 alters the oscillation frequency: a smaller value (e.g., $1.5 \times 10^{-3}\,\text{eV}^2$) lengthens L_{osc} or shifts E_{max} downward. Varying $\sin^2 2\theta$ affects only the amplitude, with lower values reducing the oscillation strength. These effects are evident in both pathlength and energy plots, highlighting the critical role of parameter tuning in neutrino studies.

Comparison to Data

Experimental data, such as from Super-Kamiokande, was initially simulated but excluded from the final plots. The theoretical predictions use vacuum oscillations, neglecting matter effects and detector efficiencies present in real data. The base $\Delta m^2 = 2.5 \times 10^{-3}\,\mathrm{eV}^2$ aligns with Super-Kamiokande's atmospheric neutrino results, but direct comparison requires experimental data beyond this analysis.

2. Three-Flavor Neutrino Oscillation Analysis

This section explores three-flavor neutrino oscillations, examining the probabilities of $\nu_\mu \to \nu_e$, $\nu_\mu \to \nu_\mu$, and $\nu_\mu \to \nu_\tau$ transitions as functions of pathlength and neutrino energy. The plots, generated using Python with Matplotlib, highlight the complex interference patterns, or "wiggles," arising from two mass-squared splittings (Δm^2_{21}, Δm^2_{31}) and three mixing angles (θ_{12}, θ_{13}, θ_{23}).

2.1 Key Equations

Three-flavor neutrino oscillations are governed by the PMNS matrix, which relates flavor eigenstates (ν_e, ν_μ, ν_τ) to mass eigenstates (ν_1, ν_2, ν_3). The oscillation probability in vacuum is:

$$P(\nu_\alpha \to \nu_\beta) =$$

$$\delta_{\alpha\beta} - 4\sum_{i>j} \mathrm{Re}(U^*_{\alpha i} U_{\beta i} U_{\alpha j} U^*_{\beta j}) \sin^2\left(\frac{1.267 \Delta m^2_{ij} L}{E_\nu}\right) + 2\sum_{i>j} \mathrm{Im}(U^*_{\alpha i} U_{\beta i} U_{\alpha j} U^*_{\beta j}) \sin\left(\frac{2.534 \Delta m^2_{ij} L}{E_\nu}\right), \tag{6}$$

where:

- U: PMNS matrix elements, parameterized by mixing angles θ_{12}, θ_{13}, θ_{23}, and CP phase δ_{CP}.
- $\Delta m^2_{ij} = m^2_i - m^2_j$: Mass-squared differences (in eV^2).
- L: Pathlength (in km).
- E_ν: Neutrino energy (in GeV).
- 1.267: Unit conversion factor.

With $\delta_{CP} = 0$, the imaginary term vanishes. The parameters used are:

- $\Delta m^2_{21} = 7.5 \times 10^{-5}\,\mathrm{eV}^2$ (solar).
- $\Delta m^2_{31} = 2.5 \times 10^{-3}\,\mathrm{eV}^2$ (atmospheric).
- $\sin^2\theta_{12} = 0.307$, $\sin^2\theta_{13} = 0.021$, $\sin^2\theta_{23} = 0.51$.

The oscillation length for each mass splitting is:

$$L_{\mathrm{osc},ij} = \frac{2.48 E_\nu}{\Delta m^2_{ij}}. \tag{7}$$

2.2 Oscillation probability vs. Pathlength

The first plot shows oscillation probabilities versus pathlength from 0 to 35 000 km with a fixed $E_\nu = 1\,\text{GeV}$.

Figure 7: Three-neutrino oscillation probabilities vs. pathlength for $\nu_\mu \to \nu_e$, $\nu_\mu \to \nu_\mu$, and $\nu_\mu \to \nu_\tau$ at $E_\nu = 1\,\text{GeV}$.

The plot exhibits rapid oscillations driven by $\Delta m^2_{31} \approx 2.5 \times 10^{-3}\,\text{eV}^2$, with an oscillation length $L_{\text{osc},31} \approx 992\,\text{km}$. Slower "wiggles" from $\Delta m^2_{21} \approx 7.5 \times 10^{-5}\,\text{eV}^2$ ($L_{\text{osc},21} \approx 33\,067\,\text{km}$) are prominent over the long baseline. The probability $P(\nu_\mu \to \nu_\tau)$ dominates, peaking near 0.8, due to the large θ_{23}, while $P(\nu_\mu \to \nu_e)$ remains small (0.02) due to small θ_{13}. The survival probability $P(\nu_\mu \to \nu_\mu)$ oscillates inversely to $P(\nu_\mu \to \nu_\tau)$.

2.3 Oscillation Probabilty vs. Energy

The second plot shows oscillation probabilities versus neutrino energy from 0.1 to 10 GeV with a fixed $L = 700\,\text{km}$.

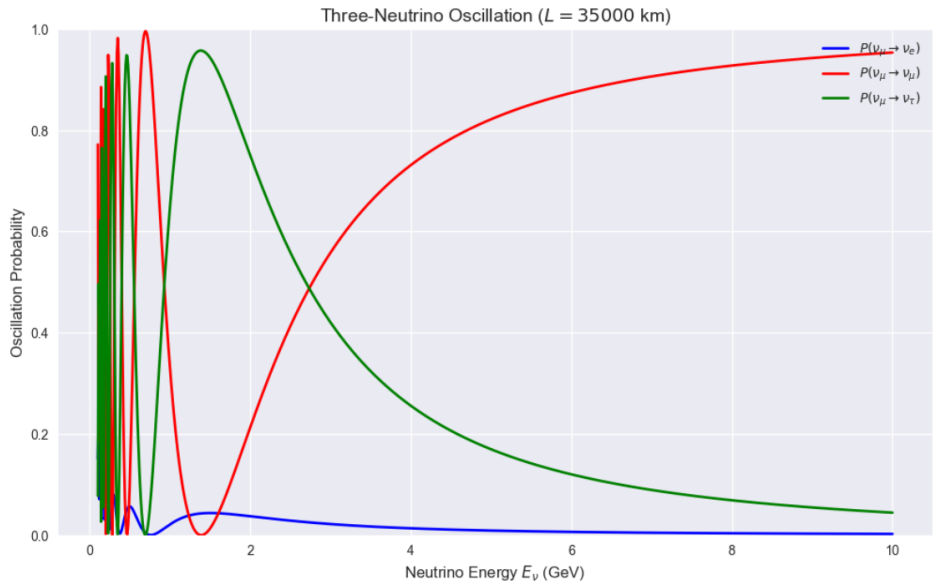

Figure 8: Three-neutrino oscillation probabilities vs. energy for $\nu_\mu \to \nu_e$, $\nu_\mu \to \nu_\mu$, and $\nu_\mu \to \nu_\tau$ at $L = 700\,\text{km}$.

At low energies (e.g., 0.1 GeV), the phase $\frac{1.267\Delta m^2_{ij} L}{E_\nu}$ is large, leading to rapid oscillations, particularly from Δm^2_{31}. As E_ν increases, oscillations slow, with fewer cycles due to the smaller phase. Wiggles from Δm^2_{21} are visible, especially at lower energies, due to the long pathlength amplifying solar effects. Similar to the pathlength plot, $P(\nu_\mu \to \nu_\tau)$ dominates, $P(\nu_\mu \to \nu_e)$ is small, and $P(\nu_\mu \to \nu_\mu)$ varies inversely to $P(\nu_\mu \to \nu_\tau)$.

Physics Insights

The oscillation patterns result from interference between three mass eigenstates, modulated by:

- **Mixing Angles**: Large $\theta_{23} \approx 45°$ enhances $\nu_\mu \to \nu_\tau$, while small $\theta_{13} \approx 8.5°$ suppresses $\nu_\mu \to \nu_e$. The angle $\theta_{12} \approx 33.5°$ influences solar-driven transitions.
- **Mass Splittings**: Δm^2_{31} drives fast oscillations, with a shorter $L_{\text{osc},31}$. Δm^2_{21} introduces slower wiggles, prominent over long baselines or at low energies.
- **Phase**: The term $\frac{1.267\Delta m^2_{ij} L}{E_\nu}$ governs oscillation frequency. Larger L or smaller E_ν increases the phase, yielding more cycles.

The long pathlength (35 000 km) amplifies both atmospheric and solar effects, making wiggles from Δm^2_{21} visible. In the energy plot, lower E_ν enhances oscillation frequency, relevant for experiments probing solar parameters.

2.4 Computational Methodology

The plots were generated using Python scripts leveraging the `numpy` library for numerical computations and `matplotlib` for visualization. The steps to produce the plots are as follows:

1. **Parameter Definition**: The oscillation parameters were set according to PDG 2020 values: $\Delta m^2_{21} = 7.5 \times 10^{-5}\,\text{eV}^2$ (solar), $\Delta m^2_{31} = 2.5 \times 10^{-3}\,\text{eV}^2$ (atmospheric), $\sin^2\theta_{12} = 0.307$, $\sin^2\theta_{13} = 0.021$, $\sin^2\theta_{23} = 0.51$, and $\delta_{CP} = 0$ (no CP violation). For the pathlength plot, the neutrino energy was fixed at $E_\nu = 1\,\text{GeV}$, and for the energy plot, the pathlength was fixed at $L = 35\,000\,\text{km}$.

2. **PMNS Matrix Construction**: The PMNS matrix was constructed using the mixing angles θ_{12}, θ_{13}, and θ_{23}, computed from their $\sin^2$ values via the arcsine function. The matrix elements were defined for all flavor transitions, accounting for the complex phase $\delta_{CP} = 0$.

3. **Probability Calculation**: The oscillation probability $P(\nu_\alpha \to \nu_\beta)$ was computed using the standard three-flavor formula (Equation 6). A custom function calculated the real part of the interference terms for each pair of mass eigenstates (i, j), summing contributions from Δm^2_{21}, Δm^2_{31}, and Δm^2_{32}. Probabilities were clipped to the physical range [0, 1] to handle numerical precision errors.

4. **Data Generation**: For the pathlength plot, a pathlength array was created from 0 to 35 000 km with 1000 points using `numpy.linspace`. For the energy plot, an energy array spanned 0.1 to 10 GeV. Probabilities were computed for $\nu_\mu \to \nu_e$, $\nu_\mu \to \nu_\mu$, and $\nu_\mu \to \nu_\tau$ at each point.

5. **Plotting**: The `seaborn-v0_8` style was applied for a professional appearance. Each plot used `matplotlib.pyplot` to draw probabilities with distinct colors (blue for ν_e, red for ν_μ, green for ν_τ). The y-axis was set to [0, 1], and a legend was placed in the upper right with a white background and black border. The plots were saved as high-resolution PNG files (`three_neutrino_oscillation_35000km.png` and `three_neutrino_oscillation_energy_35000km.png`).

3. MSW Resonance

This section examines the Mikheyev-Smirnov-Wolfenstein (MSW) effect, which enhances neutrino oscillations in matter due to interactions with electrons. I present a plot of the effective mixing parameter $\sin^2 2\theta_m$ for two-flavor neutrino mixing ($\nu_e \leftrightarrow \nu_\mu$) as a function of the dimensionless parameter $\xi = 2VE/\Delta m^2$, where $V = \sqrt{2}G_F N_e$ is the matter potential, E is the neutrino energy, and Δm^2 is the mass-squared difference. Generated using Python with the `numpy` and `matplotlib` libraries, the plot illustrates the resonance behavior for neutrinos ($\xi > 0$) and antineutrinos ($\xi < 0$) across multiple vacuum mixing angles.

3.1 Effective Mixing Angle in Matter vs. Electron Density

3.1.1 Computational Methodology

The plot was generated using a Python script leveraging the `numpy` and `matplotlib` libraries, with the `seaborn-v0_8` style for professional visualization. The computational steps are as follows:

1. **Parameter Initialization**: Three vacuum mixing angles were selected: $\sin^2\theta = 0.1$, 0.307 (PDG 2020 value for θ_{12}, relevant to solar neutrinos), and 0.5. These values span a range to demonstrate the dependence of resonance behavior on θ. The parameter $\xi = 2VE/\Delta m^2$ was defined over a range from -5 to 5 using 1000 points, created with `numpy.linspace`, to capture low-density ($\xi \to 0$), resonance, and high-density ($\xi \to \pm\infty$) regimes.

2. **Effective Mixing Angle Calculation**: For each $\sin^2\theta$, the vacuum mixing angle θ was computed as $\theta = \arcsin\left(\sqrt{\sin^2\theta}\right)$. The vacuum mixing parameter $\sin^2 2\theta = \sin^2(2\theta)$ and $\cos 2\theta$ were calculated. The effective mixing parameter in matter was computed using:
$$\sin^2 2\theta_m = \frac{\sin^2 2\theta}{(\xi - \cos 2\theta)^2 + \sin^2 2\theta}, \tag{8}$$
implemented as a Python function `sin2_2theta_m(xi, sin2_theta)`.

3. **Plotting**: The `matplotlib.pyplot` module was used to create the plot. For each $\sin^2\theta$, $\sin^2 2\theta_m$ was plotted versus ξ with distinct colors (blue for $\sin^2\theta = 0.1$, red for 0.307, green for 0.5). Dashed lines (`linestyle='--'`) marked the vacuum $\sin^2 2\theta$ for each curve, and dotted lines (`linestyle=':'`) marked the resonance condition $\xi = \cos 2\theta$. Annotations were added using `plt.annotate` to label resonance points at $\xi \approx \cos 2\theta$, with arrows pointing to the peak ($\sin^2 2\theta_m = 1$). The x-axis was labeled as $\xi = 2VE/\Delta m^2$, and the y-axis as $\sin^2 2\theta_m$, with a range of [0, 1.1].

3.1.2 Key Equations

The effective mixing angle in matter is given by:

$$\sin^2 2\theta_m = \frac{\sin^2 2\theta}{(\xi - \cos 2\theta)^2 + \sin^2 2\theta}, \tag{9}$$

where:

- θ: Vacuum mixing angle.
- $\xi = 2VE/\Delta m^2$: Dimensionless parameter, with $V = \sqrt{2}G_F N_e$ (matter potential), E (neutrino energy), Δm^2 (mass-squared difference), G_F (Fermi constant), and N_e (electron density).

The resonance condition occurs when:

$$\xi = \cos 2\theta, \tag{10}$$

yielding $\sin^2 2\theta_m = 1$ ($\theta_m = \pi/4$). The resonance width, where $\sin^2 2\theta_m > 0.5$, is:

$$\xi \in [\cos 2\theta - \sin 2\theta, \cos 2\theta + \sin 2\theta]. \tag{11}$$

Subsection for plot description

3.1.3 MSW Mixing Angle Plot

The plot displays $\sin^2 2\theta_m$ versus ξ from -4 to 4 for vacuum mixing angles $\sin^2\theta = 0.1$, 0.307, and 0.5.

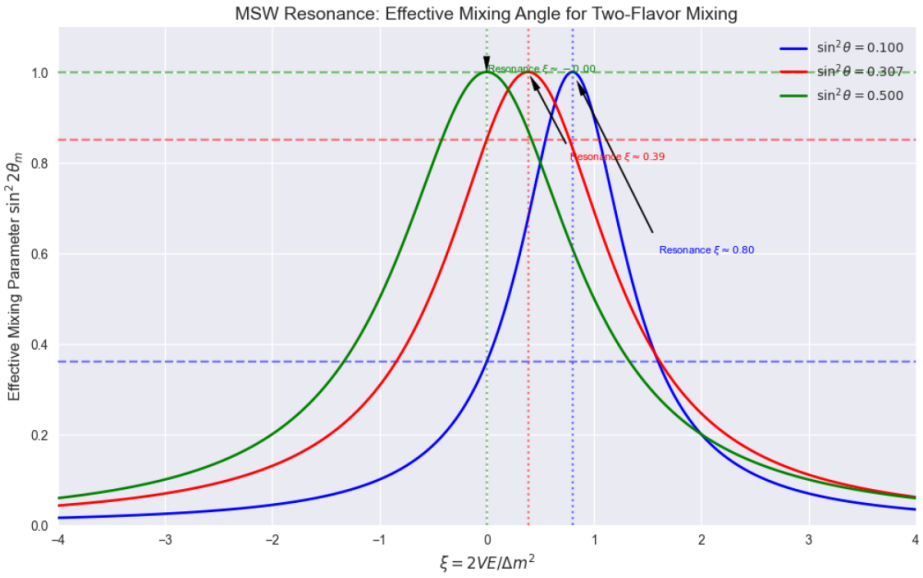

Figure 9: MSW resonance: Effective mixing parameter $\sin^2 2\theta_m$ vs. $\xi = 2VE/\Delta m^2$ for $\sin^2\theta = 0.1, 0.307, 0.5$, showing neutrinos. Dashed lines indicate vacuum $\sin^2 2\theta$, and dotted lines mark resonance at $\xi = \cos 2\theta$.

Each curve peaks at $\sin^2 2\theta_m = 1$ when $\xi = \cos 2\theta$ (e.g., $\xi \approx 0.39$ for $\sin^2\theta = 0.307$), indicating resonance. For $\xi \to 0$, $\sin^2 2\theta_m \to \sin^2 2\theta$ (vacuum limit, marked by dashed lines). For $\xi \to +\infty$ (neutrinos), $\sin^2 2\theta_m \to 0$ ($\theta_m \to \pi/2$); for $\xi \to -\infty$ (antineutrinos), $\sin^2 2\theta_m \to 0$ ($\theta_m \to 0$). Smaller θ values (e.g., $\sin^2\theta = 0.1$) result in narrower resonance widths, as seen in the plot.

The plot illustrates critical aspects of the MSW effect:

- **Low-Density Limit ($\xi \to 0$)**: The effective mixing angle approaches the vacuum value, $\sin^2 2\theta_m \to \sin^2 2\theta$, as matter effects become negligible.
- **Resonance Condition**: At $\xi = \cos 2\theta$, $\sin^2 2\theta_m = 1$, maximizing the oscillation amplitude, which is crucial for solar neutrino transitions observed in experiments like SNO and Super-Kamiokande.
- **Resonance Width**: The range where $\sin^2 2\theta_m > 0.5$ narrows with smaller θ, as evident for $\sin^2\theta = 0.1$, indicating a more pronounced resonance for smaller mixing angles.

3.2 Effective squared masses in matter for neutrinos in the case of two flavor mixing

I analyzed a key graph illustrating the effective squared masses (m^2) of neutrinos as a function of the parameter $2EV$ (in eV^2), where E is the neutrino energy and V is the matter potential. The graph, reproduced from experimental data, highlights the

resonance behavior for different vacuum mixing angles ($\sin^2 2\theta_0 = 0.1, 0.05, 0.01$). I go through the underlying equations and provide a comprehensive physical interpretation, demonstrating the MSWeffect's role in resolving the solar neutrino problem.

3.2.1 Introduction

Neutrino oscillations arise from the quantum mechanical mixing of neutrino flavor states (ν_e, ν_μ, ν_τ) due to non-zero mass differences. The MSWeffect enhances this mixing in dense media, such as the Sun, by introducing a matter potential that alters the effective mixing angles and mass eigenvalues. The provided graph (Figure 10) visually captures this effect, plotting effective squared masses against $2EV$, a parameter encapsulating the interplay between vacuum oscillations and matter effects, with a pronounced resonance where oscillation amplitudes peak.

3.2.2 Theoretical Framework

The vacuum Hamiltonian for two-flavor neutrino oscillations is:

$$H_{\text{vac}} = -\frac{\Delta m^2 \cos 2\theta_v}{4E}\sigma_3 + \frac{\Delta m^2 \sin 2\theta_v}{4E}\sigma_1,$$

where$\Delta m^2 = m_2^2 - m_1^2$ is the mass squared difference, θ_{v} is the vacuum mixing angle, E is the neutrino energy, and $\boldsymbol{\sigma_i}$ are Pauli matrices.

In matter, the Hamiltonian includes a potential $\lambda = \sqrt{2}G_F n_e$, where G_F is the Fermi constant and n_e is the electron density:

$$\mathbf{H}_{\text{matter}} = \frac{\lambda - \frac{\Delta m^2 \cos 2\theta_{\text{v}}}{2E}}{2}\boldsymbol{\sigma_3} + \frac{\Delta m^2 \sin 2\theta_{\text{v}}}{4E}\boldsymbol{\sigma_1}.$$

The matter potential $V = \lambda/\sqrt{2}$ modifies the mixing. The effective mixing angle θ_{m} and oscillation frequency ω_{m} are:

$$\tan 2\theta_{\text{m}} = \frac{\sin 2\theta_{\text{v}}}{\cos 2\theta_{\text{v}} - \frac{2EV}{\Delta m^2}},$$

$$\omega_{\text{m}} = \frac{\Delta m^2}{2E}\sqrt{\left(\frac{2EV}{\Delta m^2} - \cos 2\theta_{\text{v}}\right)^2 + \sin^2 2\theta_{\text{v}}}.$$

Resonance occurs when $\frac{2EV}{\Delta m^2} = \cos 2\theta_{\text{v}}$, maximizing $\sin^2 2\theta_{\text{m}} = 1$, enhancing oscillation probabilities.

3.2.3 Analysis of the Graph

Figure 10 plots the effective squared masses (m^2) against $2EV$ (in eV^2), where $V = \lambda/\sqrt{2}$ is the matter potential in energy units. The x-axis $2EV$ scales with the matter density and energy, providing a dimensionless measure of the MSWeffect's strength.

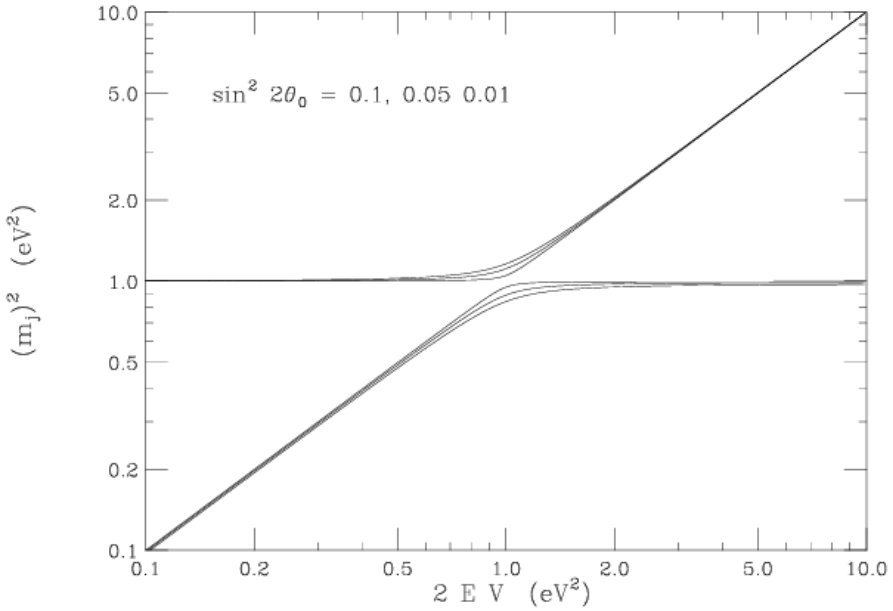

Figure 10: Effective squared masses (m^2) as a function of $2EV$ (in eV^2) for $\sin^2 2\theta_0 = 0.1, 0.05, 0.01$. The resonance is evident where the mass levels cross, minimizing the energy splitting.

Key Features

1. **Resonance Crossing**: At $2EV \approx \cos 2\theta_{\text{v}}$, the mass eigenvalues (curved lines) cross, indicating resonance. Here, the matter potential balances the vacuum term, minimizing the splitting and maximizing θ_{m}.

2. **Vacuum Limit**: As $2EV \to 0$ (high density), the masses diverge due to the matter dominance. As $2EV \to \infty$ (low density), the curves approach vacuum Δm^2, shown by the diagonal asymptote.

3. **Mixing Angle Dependence**: Larger $\sin^2 2\theta_0$ (e.g., 0.1) broadens the resonance region, as $\sin^2 2\theta_{\text{m}}$ scales with $\sin^2 2\theta_{\text{v}}$.

3.2.4 Physical Interpretation

The resonance enhances $\nu_e \to \nu_\mu$ conversion in the Sun, addressing the solar neutrino deficit (e.g., Homestake experiment). The adiabatic (meaning of which is the density

profile of matter gently reduces to vacuum, leaving enough reaction time for the neutrinos) passage through resonance converts ν_e to ν_μ or ν_τ, reducing the detected ν_e flux. The graph's curvature reflects the non-linear vacuum-matter interplay, a signature of the MSWeffect, validated by experiments like SNO and Super-Kamiokande.

3.2.5 Conclusion

The MSWeffect elegantly explains neutrino behavior in matter, as visualized in Figure 10. The resonance phenomenon, governed by the derived equations, highlights the dynamic adaptation of mass eigenvalues, offering a profound solution to the solar neutrino puzzle. This analysis underscores the MSWeffect's critical role in advancing particle physics.

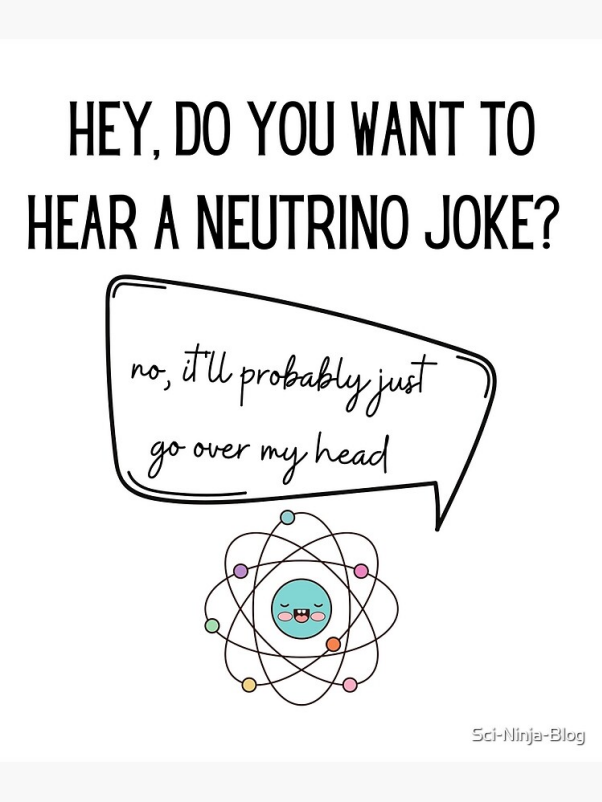

My Journey in Neutrino Physics

My fascination with neutrino physics began as a captivating exploration into the elusive world of these ghostly particles, nearly massless, chargeless, and capable of traversing vast distances through matter with minimal interaction. What started as a curiosity about the "missing" solar neutrinos, a puzzle that baffled scientists for decades, evolved into the subject. The journey has been nothing short of exhilarating, yet enjoyable.

The Python scripts used to create these plots, covering two-flavor oscillations, three-flavor oscillations, and the MSW effect basic plot, are publicly available in my GitHub repository: https://github.com/GJ-007-sage/NeutrinoPhysics.

References

[1] Lipari, P. *Introduction to Neutrino Physics*. CERN Lecture Notes. Retrieved from https://cds.cern.ch/record/677618/files/p115.pdf

[2] Uma Sankar. *Neutrino Physics*. [YouTube Playlist]. Retrieved from https://youtube.com/playlist?list=PLyhIqpk4NyE0uSw7Tv8ur6JKzOrudQKZJ&si=1oasbcnV7KgNUsfl.

[3] . *5.1. MSW Effect*. In *Neutrino Notes*. [Online Document]. Available: https://docs.neutrino.xyz/matter/msw.html

[4] AncientZygote. *neutrinos: Brief Python SciPy NumPy Matplotlib codes related to neutrino physics*. [GitHub Repository]. Retrieved from https://github.com/AncientZygote/neutrinos.